Short-period (Ga,Mn)As/(Al,Ga)As multilayer structures studied by cross-sectional scanning tunneling microscopy

S. J. C. Mauger,[1,*] M. Bozkurt,[1] P. M. Koenraad,[1] A. D. Giddings,[2] R. P. Campion,[2] and B. L. Gallagher[2]

[1]*COBRA Inter-University Research Institute, Department of Applied Physics, Eindhoven University of Technology, P.O. Box 513, NL-5600 MB Eindhoven, The Netherlands*

[2]*School of Physics and Astronomy, University of Nottingham, Nottingham, NG7 2RD, United Kingdom*

(Received 9 September 2010; revised manuscript received 12 July 2011; published 16 September 2011)

$(Ga_{1-x},Mn_x)As/GaAs$ and $(Ga_{1-x},Mn_x)As/(Al_{0.2},Ga_{0.8})As$ multilayer structures grown by molecular beam epitaxy have been studied by cross-sectional scanning tunneling microscopy. These dilute magnetic semiconductor multilayer structures have been predicted to have a strong giant magnetoresistance effect and enhanced Curie temperature. However, a sharp and short-period digital doping profile of the Mn acceptors is essential to achieve this, and therefore the studied samples were grown at a low growth temperature (250 °C). Cross-sectional scanning tunneling microscopy measurements show that the overall quality of the structure is good but many As antisites are present due to the low growth temperature. The observed Mn profile showed that, despite the low growth temperature, about 20% of the Mn acceptors from the doped layers (eight monolayers thick) end up in the nominally undoped spacer layers (four monolayers thick). This segregation puts serious constraints on the creation and application of short-period dilute magnetic superlattices because of the magnetic shortcut caused by the Mn acceptors in the spacer layer.

DOI: 10.1103/PhysRevB.84.104432 PACS number(s): 75.50.Pp, 68.65.Ac, 68.37.Ef

I. INTRODUCTION

Dilute magnetic semiconductor (DMSs) have attracted a strong scientific interest in recent years. Such materials can combine electrical, optical, and magnetic properties that can be applied, for instance, in information processing.[1] Due to the ready compatibility with current state-of-the-art of semiconductor technology and its potential for room-temperature ferromagnetism,[2–4] (Ga,Mn)As has become the model system in the Dilute magnetic semiconductor field. Theory, based on a $\boldsymbol{k}\cdot\boldsymbol{p}$ approach, has predicted that short-period (Ga,Mn)As/(Al,Ga)As superlattices with low Mn concentration allow for an antiferromagnetic interlayer exchange coupling which can give rise to giant magnetoresistance effects or spin-polarized devices.[5] Additionally, it has been predicted that these structures may exhibit enhanced Curie temperatures over that of bulk (Ga,Mn)As, potentially making short-period superlattices a route toward creating a room-temperature DMS.[6]

But, in spite of good structural properties shown by x-ray-diffraction measurements, only ferromagnetic interlayer exchange coupling has been found in similar (Ga,Mn)As/GaAs multilayer structures with undoped barriers.[7,8] The presence of Mn in the nonmagnetic layers may be the reason for the absence of an antiparallel ferromagnetic alignment across the magnetic layers. Mn can redistribute due to diffusion and segregation, which could result in a migration into the spacer layers. Particularly, segregation was shown to occur in both Mn-doped III/V materials and Mn-doped II/VI materials.[9–12] To verify this hypothesis for the (Ga,Mn)As/GaAs multilayer structures, we imaged individual Mn atoms in the cross-sectional cleavage (110) surface of the short-period superlattice in order to determine the distribution profile of Mn atoms in the growth direction.

II. EXPERIMENTAL DETAILS

The superlattices were grown by low-temperature molecular beam epitaxy (LTMBE) techniques at 250 °C, according to the design proposed by Giddings *et al.*[13] The periodic structure, deposited on a (001) semi-insulating GaAs substrate, consists of a 50 times repeated sequence of eight monolayer (MLs) (2.2 nm) of $(Ga_{1-x},Mn_x)As$ and four monolayer (1.1 nm) of either GaAs or $(Al_{0.2},Ga_{0.8})As$. The intended Mn concentration, x, in the doped layers was 2.26%; this low concentration was planned to minimize interstitial Mn and to reduce the diffusion of Mn into the barriers.[14] Samples were cleaved *in situ* under ultrahigh vacuum ($< 6 \times 10^{-11}$ mbar) and measurements were performed using a commercial room-temperature Omicron scanning tunneling microscope (STM).

Figures 1(a) and 1(b) show part of the multilayer structure and the GaAs substrate as measured by cross-sectional scanning tunneling microscopy (X-STM). The tunnel conditions were chosen at sample voltage $V_{\text{sample}} = -2$ V and a tunneling current $I = 0.04$ nA in order to achieve atomic resolution. Under these conditions, only Mn atoms in the uppermost monolayer of the (110) cross-sectional surface are imaged. Because the substrate is undoped and the multilayer structure has a p-type conductivity, due to the Mn doping, fewer states are available for tunneling out of the valence band in the GaAs substrate compared to the superlattice for the chosen tunnel conditions. Therefore, the substrate appears darker than the multilayer area. Atomic-like bright features correspond to substitutional Mn atoms,[15] whereas interstitial Mn are not visible. Dark atomic-like features are interpreted as As_{Ga} antisite defects[16] localized in the uppermost monolayer. A high concentration of As_{Ga} (0.3%) is observed, which is not surprising for the low growth temperature of 250 °C.[17]

Adsorbates are also seen, especially in Fig. 1(b). These adsorbates are present only in the multilayer part of the

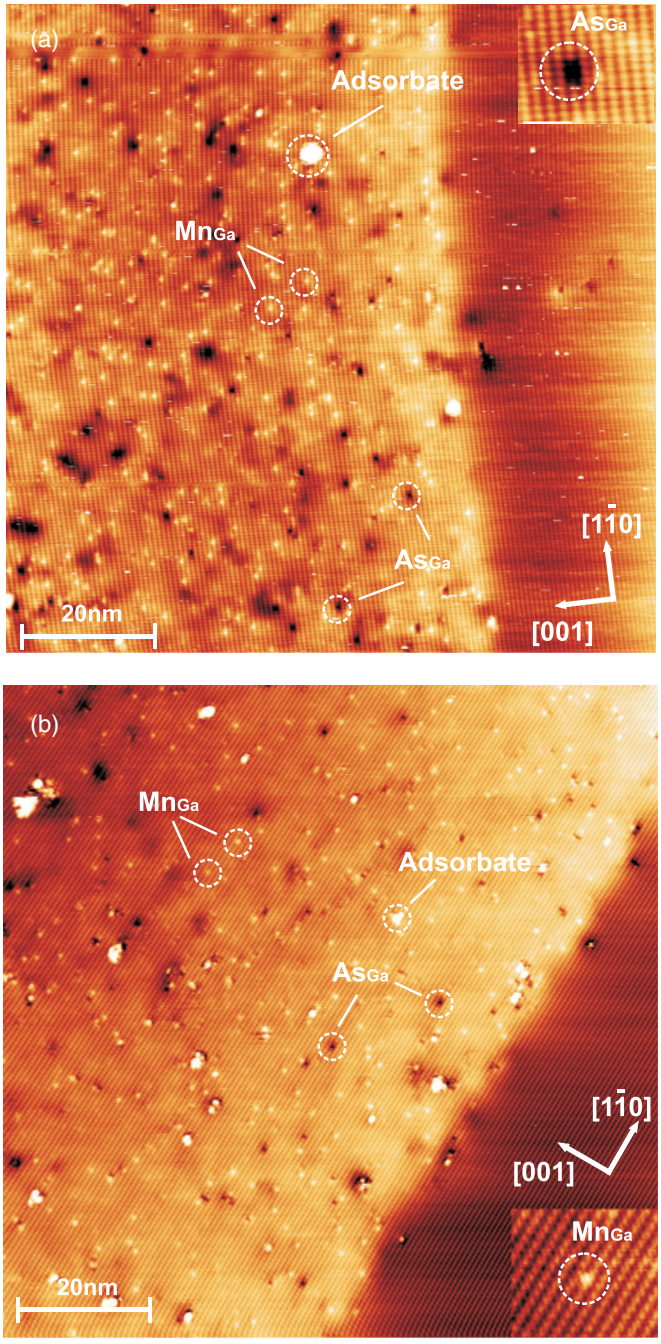

FIG. 1. (Color online) X-STM image (100×100 nm^2) of the (110) cleavage plane through the (a) $(Ga_{0.98},Mn_{0.02})As/GaAs$ superlattice structure and (b) $(Ga_{0.98},Mn_{0.02})As/(Al_{0.2},Ga_{0.8})As$ superlattice structure. Top inset is a close-up (8×7 nm^2) on a As_{Ga} defect. Bottom inset is a close-up (8×7 nm^2) on a single Mn_{Ga} impurity.

structure and their concentration is higher for the sample containing Al, which is known to be very reactive and to easily bind adsorbates. Due to the electronic contribution of ionized acceptors at negative voltage, Mn atoms appear as elevations on topographical images in constant current mode, as we can see in Fig. 2(a).

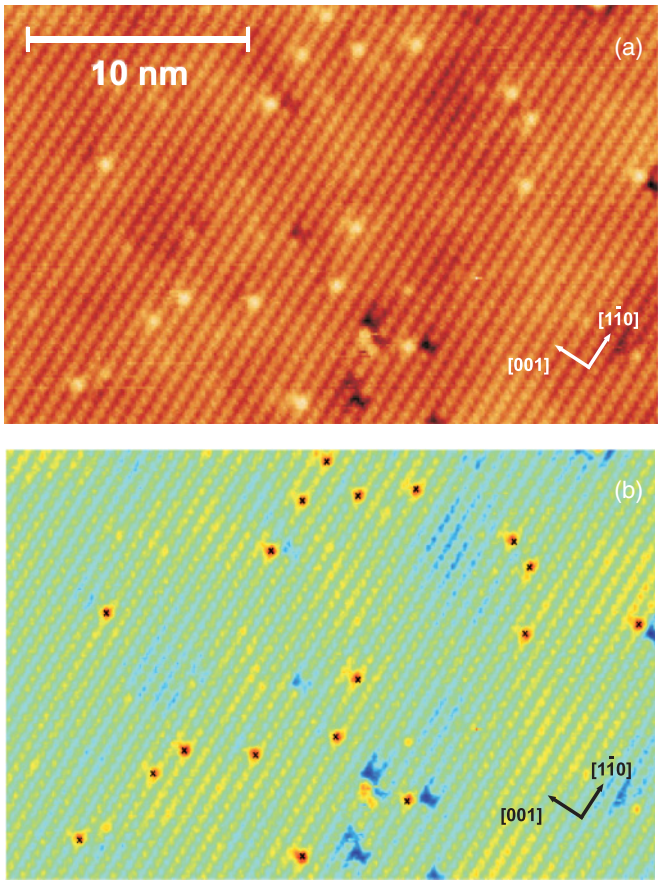

FIG. 2. (Color online) (a) Topographical X-STM image (29.3×18.8 nm^2) of the multilayer structure showing surface Mn atoms (brightest features) and As antisites (darkest features). (b) Same area as (a); black crosses show how the algorithm locates only the Mn atoms. From such a picture, the position and the number of Mn atoms along each atomic row in the [001] direction can be determined.

III. IMAGE ANALYSIS

At first sight, no periodic arrangement of the Mn atoms can be distinguished from either picture. In order to better determine if the grown structure contains a modulation in the doping distribution, the Mn distribution profile is plotted along the growth direction.

Counting of Mn atoms was realized by image analysis and Fig. 2 shows the results of this automated selection procedure. The atomic row positions, determined by automatic selection, of Mn atoms are sorted along the [001] growth direction. Counting Mn atoms in each atomic row was performed over a length of about 100 nm perpendicular to the growth direction.

The distribution profiles obtained from the X-STM measurements of Figs. 1(a) and 1(b) are shown in Figs. 3(a) and 3(b). From these distributions, the estimation of the average Mn concentration in the multilayer is equal to $x = 1.1\%$ and $x = 1.2\%$ for the $(Ga_{0.98},Mn_{0.02})As/GaAs$ and $(Ga_{0.98},Mn_{0.02})As/(Al_{0.2},Ga_{0.8})As$ samples, respectively. The growth conditions were chosen with the intention of achieving a Mn doping of 2.26% in the eight ML thick magnetic layers. Taking account of the periodic structure, which also includes spacer layers with a thickness of four

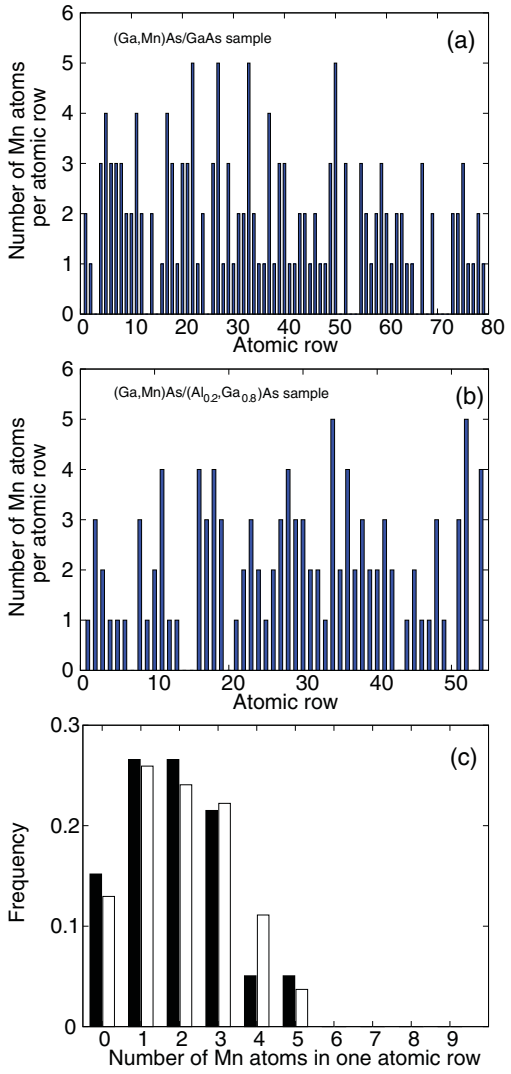

FIG. 3. (Color online) (a) and (b) represent the number of Mn atoms present in each atomic row along the [001] growth direction for, respectively, the $(Ga_{0.98},Mn_{0.02})As/GaAs$ superlattice structure and the $(Ga_{0.98},Mn_{0.02})As/(Al_{0.2},Ga_{0.8})As$ superlattice structure. (c) shows the frequency distribution $f(k)$ for the number of rows, of length 100 nm, perpendicular to the growth direction, which contain k Mn atoms obtained from the data of Figs. 3(a) (filled histogram) and 3(b) (open histogram).

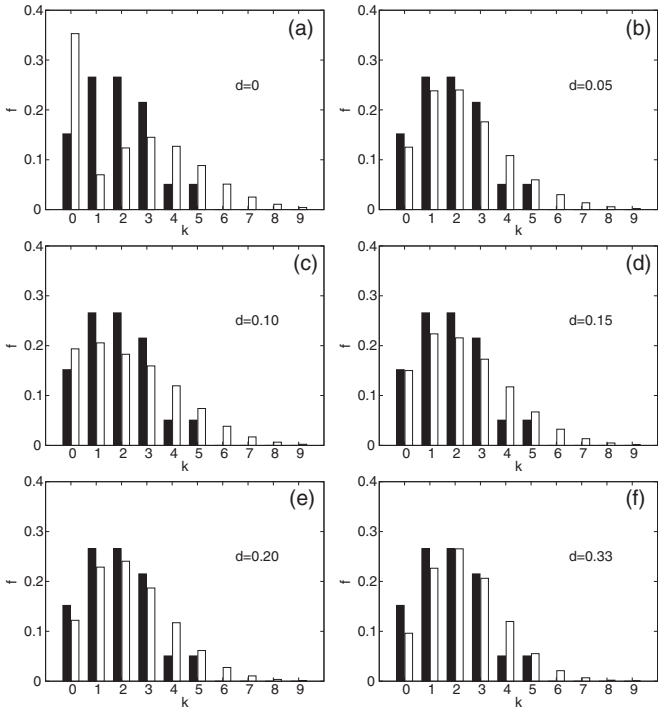

FIG. 4. The histograms represent the probability of finding atomic rows which contain $0,1,2,3\ldots$ Mn atoms over a length of 100 nm. The filled histogram is the experimentally obtained distribution also shown in Fig. 3(a) ($x = 0\%$), whereas the open histograms are simulated distributions of multilayer structures where a fraction d of Mn atoms of the magnetic layers has ended up in the spacer layer. (a) $d = 0$ corresponds to an ideal superlattice, (b) $d = 0.05$, (c) $d = 0.10$, (d) $d = 0.15$, (e) $d = 0.20$, and (f) $d = 0.33$ corresponds to bulk (Ga,Mn)As, where Mn atoms are uniformly distributed.

MLs, the bulk concentration averaged over all the layers is expected to be 1.5%. This value is close to the experimentally observed concentration. The small difference between the intended and the measured concentration might be related to the calibration of the Mn flux during the growth or the difficulties in identifying all Mn atoms via our automated image analysis. From the histograms shown in Figs. 3(a) and 3(b), it is still difficult to distinguish a periodicity. Figure 3(c) shows the frequency distribution $f(k)$ for the number of rows perpendicular to the growth direction which contain k Mn atoms obtained from the data of Figs. 3(a) and 3(b). Both distributions are centered on $k = 2$ and have the same width. This suggests that Al has no effect on the Mn distribution. Figure 4 shows a comparison between $f(k)$ obtained from the data of Fig. 3(a) (filled histogram) and simulations (open histogram) for various degrees of Mn redistribution.

Figure 4(a) shows a comparison with an ideal superlattice in which Mn atoms are only found in the magnetic layers and not in the spacer layers. Figure 4(f) shows a comparison with a homogeneous Mn concentration in the growth direction. Figures 4(b)–4(e) are intermediate cases in which a fraction d of, respectively, 5%, 10%, 15%, and 20% of Mn atoms has diffused or segregated into the nonmagnetic layers.

IV. DISTRIBUTION MODEL

For a homogeneous distribution along the growth direction, the probability, f, of finding exactly k Mn atoms in one atomic row corresponds to a binomial distribution, where n, the number of observations, corresponds to the total number of atoms in one atomic row, and p, the probability of finding a Mn atom per atomic row, corresponds to the Mn concentration. In our case, the Mn concentration was chosen to be equal to the concentration measured from Fig. 3(a), namely, $p = 1.1\%$, and $n = 178$.

$$f(k,n,p) = \frac{n!}{k!(n-k)!}\, p^k\,(1-p)^{1-k}, \quad k = 0,1,2,\ldots,n. \quad (1)$$

Furthermore, in order to simulate the same distribution for a superlattice, the previous expression is modified to take into consideration a heterogeneous Mn concentration. Following the design of the multilayer structure, the ratio between the thickness of magnetic layers and nonmagnetic layers is taken as 2 to 1, with p_M the Mn concentration in the magnetic layers and p_N the Mn concentration in the spacer layers.

$$f(k,n,p_M,p_N) = \frac{2}{3}\frac{n!}{k!(n-k)!}\,p_M^k\,(1-p_M)^{1-k} + \frac{1}{3}\frac{n!}{k!(n-k)!}\,p_N^k\,(1-p_N)^{1-k}, \quad k = 0,1,2,\ldots,n \tag{2}$$

$$p_M = \tfrac{3}{2}(1-d)p, \qquad p_N = 3dp. \tag{3}$$

Equation (3) shows the definition of the concentrations p_M and p_N. The parameter d, representing the fraction of Mn in the spacer layer, can be altered in order to simulate different levels of Mn redistribution. $d = 0$ represents the case of an ideal superlattice with no Mn in the spacer, while $d = 0.33$ represents the case with a uniform Mn doping in all layers.

The simulations show that for an ideal superlattice [c*f*. Fig. 4(a)] there are two peaks in the distribution appearing at $k = 0$ and $k = 3$, which means that, in the case of an ideal superlattice with a Mn concentration about $x = 2.3\%$, it is most probable to find atomic rows with either no Mn atoms or 3 Mn atoms in the length of 100 nm that we analyzed. When simulating an increase of Mn segregation in the spacer layers, the two peaks of the distribution tend to merge and center around $k = 2$. For a bulk (Ga,Mn)As sample with an homogeneous distribution of Mn, approximately 2 Mn atoms are expected in the length of 100 nm. Both measured samples have their distribution centered around $k = 2$ and the frequency of atomic rows without Mn atoms is rather low. From careful comparison between the measured distribution and the range of simulated distributions representing either an ideal doped superlattice, bulk doped (Ga,Mn)As, or the several intermediate cases, it appears that the shape of the measured distribution is closest to the shape of the simulated distribution for $d = 0.20$. Therefore, we conclude that a periodic distribution is observed but a fraction of about 20% of the Mn deposited in the doped layers has ended up in the nonmagnetic layers.

V. DISCUSSION

In the theoretical predictions for antiferromagnetic interlayer coupling in short-period DMS superlattices, it has always been assumed that no magnetic impurities are present in the spacer layers.[13,18] Experimental work on (Ga,Mn)As-based multilayers and superlattices with spacer layers greater than 3 nm has found evidence of both ferromagnetic[7] and antiferromagnetic[8,19] interlayer exchange coupling (IEC). Polarized neutron reflectivity measurements of multilayers consisting of two (Ga,Mn)As layers separated by a GaAs spacer showed evidence of strong coupling between the two layers when the spacer is 6 nm thick, with the IEC increasing in strength for a 3 nm spacer. Mn diffusion is expected to be 1.5 nm or less[10] and thus the thick spacer layer will contain little Mn. This means the coupling will not be the result of a ferromagnetic short between the two layers. Instead this suggests that the IEC is mediated by carriers through a mechanism such as Ruderman-Kittel-Kasuya-Yosida (RKKY)-like ferromagnetic exchange or an overlap of the wave functions of holes in the two layers.[7] Although in RKKY theory one of the terms describing the coupling strength becomes greater as the spacer thickness is reduced, there is also an oscillatory term that can change the sign of the coupling between ferromagnetic and antiferromagnetic. In that study there was no indication of this oscillatory behavior, as only ferromagnetic coupling was reported.

However, antiferromagnetic coupling has been found in GaMnAs-based superlattices[8] and trilayers[19] where the nonmagnetic spacer was doped with Be, increasing the hole concentration in the spacer. In this case the AFM coupling was observed when the spacers were doped with Be whilst when the spacer was undoped, the magnetic layers were either ferromagnetically coupled or not magnetically coupled. In these studies the width of the spacer is again greater than 3 nm, although for larger spacers the AFM coupling disappears. This again suggests that the interlayer coupling is being mediated by carriers in the nonmagnetic spacer.

VI. MAGNETIC PROPERTIES

In order to analyze the magnetic properties of our short-period superlattices, superconducting quantum interference device (SQUID) magnetometry was used to measure a series of samples with different concentrations of Al in the 1.1 nm spacer layer. As can be seen from the $M(H)$ loops in Fig. 5, there is no evidence of any antiferromagnetic (AFM) IEC: the square hysteresis shape with fast magnetization reversal at the coercive field is typical for a ferromagnetic material. If there was a strong antiferromagnetic coupling then, as the magnetic field is reduced, the measured net magnetic moment would be expected to decrease as the magnetization

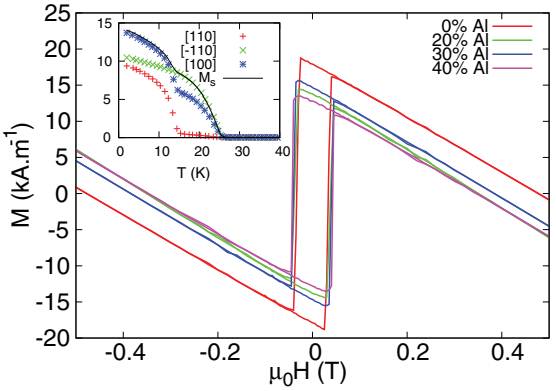

FIG. 5. (Color online) $M(H)$ hysteresis loops at $T = 2$ K for $(Al_z,Ga_{z-1})As$ superlattices with the magnetic field aligned along the cubic easy magnetic axis. The Al concentration, z, is varied between 0% and 40%. The inset shows the temperature-dependent remnant magnetization after a 1 T field has been applied along the principle crystalline axes of the $(Al_{0.2},Ga_{0.8})As$ superlattice. The calculated spontaneous magnetization, M_S, is plotted alongside.

of adjacent layers rotate in to antiparallel alignments. It is possible that all the magnetic layers are uncoupled, rather than being ferromagnetically coupled. However, in such a case, it might be expected that the magnetization reversal would not occur simultaneously as individual layers may have different coercive fields due to inhomogeneities in the layers. As a result, the switching would be ragged, occurring over a range of applied fields. This is not observed; the magnetization reversal seems to occur cohesively, indicating that the material is behaving as a single ferromagnet rather than an ensemble of many ferromagnetic layers.

Further evidence that these short-period superlattices are acting as a single ferromagnetic is given by the remnant magnetization data in the inset of Fig. 5. The good agreement between the calculated spontaneous magnetization $M_S^2 = M_{[110]}^2 + M_{[1\bar{1}0]}^2$ and the easy cubic remanent magnetization $M_{[100]}$ suggests the sample is acting as a single domain with a Curie temperature of 25 K. Given the sizable concentration of Mn in the spacer layers observed by cross-sectional scanning tunneling microscopy (X-STM), we believe that the magnetic layers are ferromagnetically shorted by the Mn and thus the sample behaves like a single ferromagnetic material rather than a multilayer.

VII. CONCLUSION

Although previous studies[9,10] have claimed that Mn does not diffuse or segregate within two to three monolayer in GaAs below a growth temperature of 400 °C, our data clearly show that Mn can move out of the magnetic layers into the spacer layer even for structures grown at a temperature as low as 250 °C. Classical diffusion can be excluded as the mechanism responsible for the redistribution of Mn because of the low growth temperature.[14] Moreover, measurements performed by Bozkurt *et al.*[20] have shown that Mn segregation occurs in GaAs for structures grown at 350 °C. Due to the high Mn concentration in the magnetic layers leading to a high two-dimensional (2D) carrier concentration $N_{2D} \approx 1 \times 10^{15}$ cm^{-2}, another possible mechanism for the redistribution of Mn could be drift resulting from the Coulomb repulsion between the ionized dopant.[21,22] In conclusion, from the cross-sectional scanning tunneling microscopy (X-STM) measurements a periodic Mn distribution in our short-period 2.2 nm/1.1 nm $(Ga_{1-x},Mn_x)As$/(Al,Ga)As superlattices was observed with a reduced amplitude due to segregation of Mn from the doped layers into the undoped layers. These magnetic impurities within the spacer layers may be the reason for the absence of interlayer exchange coupling in the short-period superlattices. The high concentrations of Mn in the spacer layers act as magnetic shorts, mediating ferromagnetism between the ferromagnetic layers. We suggest that the concept of a short-period superlattice may not be valid considering the atomistic and discrete nature of Mn atoms in these thin and low-density (Ga,Mn)As layers.

ACKNOWLEDGMENTS

The research leading to these results has received funding from the European Community's Seventh Framework Programme (PF7/2007-2013) under Grant agreement No. 215368.

*s.j.c.mauger@tue.nl

[1] G. A. Prinz, Science **282**, 1660 (1998).
[2] H. Ohno, Science **281**, 951 (1998).
[3] Y. Ohno, D. K. Young, B. Beschoten, F. Matsukura, H. Ohno, and D. D. Awschalom, Nature **402**, 790 (1999).
[4] A. H. MacDonald, P. Schiffer, and N. Samarth, Nat. Mater. **4**, 195 (2005).
[5] T. Jungwirth, W. A. Atkinson, B. H. Lee, and A. H. MacDonald, Phys. Rev. B **59**, 9818 (1999).
[6] I. Vurgaftman and J. R. Meyer, Phys. Rev. B **64**, 245207 (2001).
[7] B. J. Kirby, J. A. Borchers, X. Liu, Z. Ge, Y. J. Cho, M. Dobrowolska, and J. K. Furdyna, Phys. Rev. B **76**, 205316 (2007).
[8] J.-H. Chung, S. J. Chung, S. Lee, B. J. Kirby, J. A. Borchers, Y. J. Cho, X. Liu, and J. K. Furdyna, Phys. Rev. Lett. **101**, 237202 (2008).
[9] A. M. Nazmul, S. Sugahara, and M. Tanaka, J. Cryst. Growth **251**, 303 (2003).
[10] R. Mattana, M. Elsen, J.-M. George, H. Jaffrès, F. N. Van Dau, A. Fert, M. F. Wyczisk, J. Olivier, P. Galtier, B. Lépine, A. Guivarc'h, and G. Jézéquel, Phys. Rev. B **71**, 075206 (2005).
[11] J. A. Gaj, W. Grieshaber, C. Bodin-Deshayes, J. Cibert, G. Feuillet, Y. Merle d'Aubigné, and A. Wasiela, Phys. Rev. B **50**, 5512 (1994).
[12] W. Grieshaber, J. Cibert, J. A. Gaj, Y. Merle d'Aubigné, and A. Wasiela, Phys. Rev. B **50**, 2011 (1994).
[13] A. D. Giddings, T. Jungwirth, and B. L. Gallagher, Phys. Rev. B **78**, 165312 (2008).
[14] D. DeSimone, C. E. C. Wood, and J. C. A. Evans, J. Appl. Phys. **53**, 4938 (1982).
[15] A. M. Yakunin, A. Yu. Silov, P. M. Koenraad, J. H. Wolter, W. Van Roy, J. De Boeck, J.-M. Tang, and M. E. Flatté, Phys. Rev. Lett. **92**, 216806 (2004).
[16] R. M. Feenstra, J. M. Woodall, and G. D. Pettit, Phys. Rev. Lett. **71**, 1176 (1993).
[17] A. Wolos, M. Kaminska, M. Palczewska, A. Twardowski, X. Liu, T. Wojtowicz, and J. K. Furdyna, J. Appl. Phys. **96**, 530 (2004).
[18] K. Szałowski and T. Balcerzak, Phys. Rev. B **79**, 214430 (2009).
[19] J. Leiner, H. Lee, T. Yoo, S. Lee, B. J. Kirby, K. Tivakornsasithorn, X. Liu, J. K. Furdyna, and M. Dobrowolska, Phys. Rev. B **82**, 195205 (2010).
[20] M. Bozkurt, V. A. Grant, J. M. Ulloa, R. P. Campion, C. T. Foxon, J. E. Marega, G. J. Salamo, and P. M. Koenraad, Appl. Phys. Lett. **96**, 042108 (2010).
[21] P. M. Koenraad, M. B. Johnson, H. W. M. Salemink, W. C. van der Vleuten, and J. H. Wolter, Mater. Sci. Eng. B **35**, 485 (1995).
[22] N. S. Averkiev, A. M. Monakhov, A. Shik, P. M. Koenraad, and J. H. Wolter, Phys. Rev. B **61**, 3033 (2000).